Theses and Dissertations   1. Thesis and Dissertation Collection, all items

2010-12

Feasibility of underwater friction stir welding of hardenable alloy steel

Overfield, Norman E.

Monterey, California. Naval Postgraduate School

http://hdl.handle.net/10945/5092

NAVAL POSTGRADUATE SCHOOL

MONTEREY, CALIFORNIA

THESIS

FEASIBILITY OF UNDERWATER FRICTION STIR WELDING OF HARDENABLE ALLOY STEEL

by

Norman E. Overfield

December 2010

Thesis Advisor:	Terry R. McNelley
Second Reader:	Sarath Menon

THIS PAGE INTENTIONALLY LEFT BLANK

REPORT DOCUMENTATION PAGE		*Form Approved OMB No. 0704-0188*

Public reporting burden for this collection of information is estimated to average 1 hour per response, including the time for reviewing instruction, searching existing data sources, gathering and maintaining the data needed, and completing and reviewing the collection of information. Send comments regarding this burden estimate or any other aspect of this collection of information, including suggestions for reducing this burden, to Washington headquarters Services, Directorate for Information Operations and Reports, 1215 Jefferson Davis Highway, Suite 1204, Arlington, VA 22202-4302, and to the Office of Management and Budget, Paperwork Reduction Project (0704-0188) Washington DC 20503.

1. AGENCY USE ONLY *(Leave blank)*	2. REPORT DATE December 2010	3. REPORT TYPE AND DATES COVERED Master's Thesis	
4. TITLE AND SUBTITLE Feasibility of Underwater Friction Stir Welding of Hardenable Alloy Steel		**5. FUNDING NUMBERS**	
6. AUTHOR(S) Norman E. Overfield			
7. PERFORMING ORGANIZATION NAME(S) AND ADDRESS(ES) Naval Postgraduate School Monterey, CA 93943-5000		**8. PERFORMING ORGANIZATION REPORT NUMBER**	
9. SPONSORING /MONITORING AGENCY NAME(S) AND ADDRESS(ES) N/A		**10. SPONSORING/MONITORING AGENCY REPORT NUMBER**	

11. SUPPLEMENTARY NOTES The views expressed in this thesis are those of the author and do not reflect the official policy or position of the Department of Defense or the U.S. Government.

12a. DISTRIBUTION / AVAILABILITY STATEMENT Approved for public release; distribution is unlimited.	12b. DISTRIBUTION CODE A

13. ABSTRACT (maximum 200 words)

The objective of this thesis is to determine whether friction stir welding (FSW) is a feasible welding process for steels in an underwater environment. Specific benefits would be underwater weld repairs on steel alloy piping systems and/or structures, and crack repairs on control surfaces of submarines without the need for strict environment controls or in the submarine's case, for drydocking.

A single tool made of polycrystaline cubic boron nitride (PCBN) with a Tungsten-Rhenium binder was used to conduct a series of bead-on-plate FSW traverses, approximately 64 inches (1.6 m) in total length, on 0.25 inch (6.4 mm) thick plates of a hardenable alloy steel. The first series of traverses involved various revolutions per minute (RPM) and inches per minute (IPM) combinations on a dry plate. A second series was conducted while a plate was immersed in water in order to assess the potential for inducing hydrogen assisted cracking (HAC) during FSW of susceptible alloys. All traverses were visually defect-free. The FSW nuggets (stir zone) exhibited refined microstructures and increased hardness relative to the base plate.

Based on preliminary findings, FSW of hardenable alloy steel is a feasible process and should be further researched and refined.

14. SUBJECT TERMS Friction Stir Welding, Underwater, High Strength Steel, Microstructural Properties, Hardenable Alloy Steel, Weld Repair			**15. NUMBER OF PAGES** 55
			16. PRICE CODE
17. SECURITY CLASSIFICATION OF REPORT Unclassified	**18. SECURITY CLASSIFICATION OF THIS PAGE** Unclassified	**19. SECURITY CLASSIFICATION OF ABSTRACT** Unclassified	**20. LIMITATION OF ABSTRACT** UU

THIS PAGE INTENTIONALLY LEFT BLANK

**FEASIBILITY OF UNDERWATER FRICTION STIR WELDING OF
HARDENABLE ALLOY STEEL**

Norman E. Overfield
Lieutenant, United States Navy
B.S.M.E., Old Dominion University, 2001

Submitted in partial fulfillment of the
requirements for the degree of

MASTER OF SCIENCE IN MECHANICAL ENGINEERING

from the

**NAVAL POSTGRADUATE SCHOOL
December 2010**

Author: Norman E. Overfield

Approved by: Terry R. McNelley
                    Thesis Advisor

                    Sarath Menon
                    Second Reader

                    Knox Millsaps
                    Chairman, Department of Mechanical and Aerospace Engineering

iii

THIS PAGE INTENTIONALLY LEFT BLANK

ABSTRACT

The objective of this thesis is to determine whether friction stir welding (FSW) is a feasible welding process for steels in an underwater environment. Specific benefits would be underwater weld repairs on steel alloy piping systems and/or structures, and crack repairs on control surfaces of submarines without the need for strict environment controls or in the submarine's case, for drydocking.

A single tool made of polycrystalline cubic boron nitride (PCBN) with a Tungsten-Rhenium binder was used to conduct a series of bead-on-plate FSW traverses, approximately 64 inches (1.6 m) in total length, on 0.25 inch (6.4 mm) thick plates of a hardenable alloy steel. The first series of traverses involved various revolutions per minute (RPM) and inches per minute (IPM) combinations on a dry plate. A second series was conducted while a plate was immersed in water in order to assess the potential for inducing hydrogen assisted cracking (HAC) during FSW of susceptible alloys. All traverses were visually defect-free. The FSW nuggets (stir zone) exhibited refined microstructures and increased hardness relative to the base plate.

Based on preliminary findings, FSW of hardenable alloy steel is a feasible process and should be further researched and refined.

THIS PAGE INTENTIONALLY LEFT BLANK

TABLE OF CONTENTS

THIS PAGE INTENTIONALLY LEFT BLANK

LIST OF FIGURES

LIST OF TABLES

THIS PAGE INTENTIONALLY LEFT BLANK

LIST OF ACRONYMS AND ABBREVIATIONS

BM – Base Material

CNC – Computer Numerical Controlled

EDM – Electrical Discharge Machining

FSP – Friction Stir Processing

FSW – Friction Stir Welding

FSW/P – Friction Stir Welding and/or Processing

HAC – Hydrogen Assisted Cracking

HAZ – Heat Affected Zone

IPM – Inches per Minute

NPS – Naval Postgraduate School

PCBN – Polycrystalline Cubic Boron Nitride

RPM – Rotations per Minute

SEM – Scanning Electron Microscope

SZ – Stir Zone

TMAZ – Thermo-Mechanically Affected Zone

USN – United States Navy

THIS PAGE INTENTIONALLY LEFT BLANK

ACKNOWLEDGMENTS

THIS PAGE INTENTIONALLY LEFT BLANK

I. INTRODUCTION

Many high-strength steels are strengthened by martensitic transformation and such steels are potentially very susceptible to Hydrogen Assisted Cracking (HAC) [1]. Therefore, they require extensive preparations prior to, during, and after welding. These preparations include, but are not limited to: preheating, humidity/moisture control, filler electrode controls (testing, baking and storage), and post-heating. To weld these steels underwater is difficult and requires enclosures and special welding techniques that increase the time and costs involved for the weld [2].

Several Los Angeles class submarines have been found to have fatigue cracks in their control surfaces and have had their repairs conducted while in drydock. Even while in drydock, maintaining a dry welding environment has been difficult due to trapped moisture inside of the control surface being repaired. Every day of delay while in drydock costs the Navy, and therefore the taxpayers, tens - if not hundreds of thousands of dollars.

Friction stir welding (FSW) and the allied technique of friction stir processing (FSP) are solid state processes used in joining or processing, respectively. Applications include joining of aluminum structural components in the Littoral Combat Ship (LCS) and processing of the nickel aluminum bronze used in U.S. Navy propellers. In friction stir welding, a cylindrical, rotating tool with a shoulder and projecting pin is pressed into the surface along the abutting edges of the materials to be welded. Through frictional and adiabatic heating the material is softened enough for the tool pin to plunge into the material until the shoulder contacts the surface. The tool then transverses along the line contact to produce a weld by the localized severe plastic deformation in the resulting stir zone. Figure 1 illustrates the basic nomenclature used in FSW/P. To date, some detailed studies on the effects of friction stir welding of hardenable alloy steels have been carried out, but none for welding of them while in water.
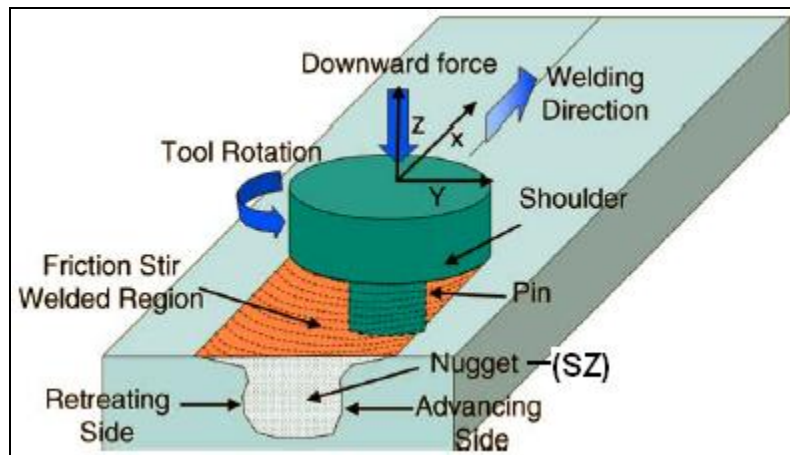
Figure 1.   FSW/P Nomenclature. After [3]

Though invented in 1991 by TWI of Cambridge, U.K., FSW/P of steels has predominantly been accomplished over the last decade due to limitations in material selection for the welding/processing tool itself. As more advanced techniques of materials processing/fabrication are developed, made commercially viable, and more robust tools are designed, FSW/P of steels becomes more economically feasible. Even so, due to the many well-established welding processes for steels added to the relative ease of welding steels compared to non-ferrous alloys, FSW/P of steels most likely will not supplant traditional methods for typical applications. However, when one considers specific applications or more restrictive welding environments, there may be areas where FSW/P of steels will be the best choice.

Hydrogen solubility will be reduced relative to processes involving temperatures above the melting point because FSW/P does not involve melting. Furthermore, the production of hydrogen through decomposition of the water molecule is not expected during FSW/P. It is this combination of FSW properties that could lead to FSW of hardenable alloy steels underwater to not only produce defect-free welds, but also to be cost effective.

II. BACKGROUND

Studies involving FSW/P of steels have been steadily increasing over the last decade, as advances in tool materials and design are made. FSW/P experiments ranging from ultralow carbon through ultrahigh carbon steels [4, 5] have demonstrated defect-free welds. FSW/P of specialized steels such as DP980 (advanced high-strength steel) [6] and SKD61 tool steel [7] have also produced defect-free welds.

The resultant microstructures of FSW/P steels are highly dependent upon the chemical composition of the base material as well as on the FSW/P tool parameters such as RPM, IPM, and Z-axis (normal) force. Parameters ranging from 1000 RPM/15 mm/s (35 IPM) [8] to 100 RPM/25 mm/min (1 IPM) [9] have produced defect-free welds. While Z-axis force parameters have not been consistently reported, they range from 5 kN (1124 lbf) [8] to 40 kN (9000 lbf) [10]. These values demonstrate that each specific type of steel will have its own set of parameters that will yield defect-free welds. As such, detailed studies will be required to determine these "operating windows" such that as long as the processing parameters are maintained within the "operating window", it can be expected that a defect-free weld will be produced.

In most cases of FSW/P of steels, a martensitic microstructure was developed in the SZ and to a lesser extent, in the TMAZ of the weld/processed beads. For these cases, the temperature in the SZ exceeded A_1 (complete austenite formation temperature) during processing and subsequently experienced rapid cooling, and therefore, formed martensite. In one study [11], martensite-free welds were produced by controlling FSW parameters and preventing the SZ temperature from exceeding A_1. These studies show that post-weld metallurgical properties can be controlled through adjusting FSW/P parameters and can therefore be modified to suit a wide range of applications and eliminate the need for pre or post-weld heat treatments.

To date, no studies have evaluated FSW/P of steels underwater. This unique environment poses particular restrictions to the conventional welder using fusion techniques and can be very costly or impractical. U.S. Navy shipyards typically do not

have qualified welders to perform any underwater welding, and there are no industry standards to weld HY-80/100 underwater [12]. HY-80/100 are alloy steels involving heat treatment to produce tempered martensitic microstructures. These materials are therefore susceptible to HAC and the possibility of using FSW/P to avoid HAC in these hardenable alloy steels formed the basis of this research. FSW/P of this type of hardenable alloy steel could provide for substantial savings by preventing the need for drydocking a submarine. As such, this study was initiated as a preliminary study to examine the feasibility of successful underwater FSW/P of steels. A hardenable alloy steel was obtained and a comparative study of dry vs. underwater FSW/P was carried out to understand the influence of several RPM/IPM combinations on the resulting microstructures and mechanical properties.

III. EXPERIMENTAL PROCEDURE

A. MATERIAL PROCESSING

A steel plate 0.25 in (6.4 mm) in thickness was acquired from the Naval Surface Warfare Center – Carderock Division. This plate was approximately 30 in (750 mm) in length and 15 in (380 mm) wide. Post-welding analysis for general chemistry revealed that its composition was closest to AISI 4142 steel. This material was cut to yield two separate plates, one to perform dry FSP beads and one to perform wet (underwater) FSP beads. The FSP was conducted at MegaStir Technologies in Provo, UT. The underwater plate was held under water by use of a two inch high sealed acrylic box over half of the plate at a time. Cooling was supplied to the water box via copper tubing that was supplied with refrigerated water. Water temperatures were monitored in the water box and ranged from the starting ambient temperature of 21°C to a high of 70°C. Several RPM/IPM combinations were examined. The FSP bead lengths were approximately eight inches (20 cm) each, for a total of 64 inches (1.6 m) of tool use. Each plate had one FSP bead that had to be discounted due to either insufficient or excessive Z-axis force that caused irregular beads. The RPM/IPM combinations for these defective beads were used again with a more refined Z-axis force and produced visually defect-free beads. Figure 2 shows in-process photos of FSP underwater. Table 1 shows the RPM/IPM combinations with other pertinent data for each FSP bead.

| Start of 400-2 FSP underwater | Close-up of tool – note boiling water |

Figure 2.   FSP at 400 RPM and 2 IPM (51 mm/min) while underwater.

Table 1. FSP Parameters.

RPM	IPM		Dry or Wet	Max. Tool Temp.		Max. Z-axis Force		Set Z-axis Force	
(rev/min)	(in/min)	(mm/min)	(D or W)	(°F)	(°C)	(lbf)	(kN)	(lbf)	(kN)
200	4	102	D	1407	764	8098	36.0217	8000	35.5858
200	4	102	W	262	128	12087	53.7657	12000	53.3787
300	4	102	D	1675	913	8490	37.7654	8000	35.5858
300	4	102	W	622	328	8103	36.0439	7000	31.1376
400	2	51	D	1780	971	8045	35.7859	8000	35.5858
400	2	51	W	657	347	8453	37.6008	8000	35.5858

The tool material was polycrystalline cubic boron nitride (PCBN) embedded in a tungsten-rhenium (W-Re) binder. The material is termed Q-70. The tool was used on a FSW/P machine in load-control operation. Figure 3 shows the PCBN tool prior to and after six FSP beads (approximately 48 inches (1.2 m)) were completed.

Before   After (6 of 8 20-cm beads)
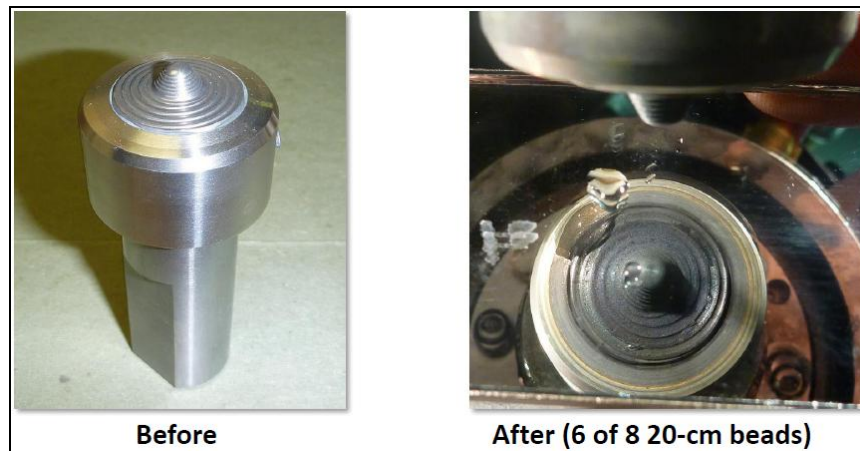
Figure 3. PCBN tool before and after FSP beads on 4142 steel plate.

B.   CHEMICAL TESTING

Luvak Inc. performed chemical testing on the BM to determine its composition, as well as hydrogen content from BM, FSP (dry) and FSP (wet) material. The 400-2 RPM/IPM combination was evaluated for FSP hydrogen content. This selection was based on its RPM/IPM combination giving the maximum heat input and therefore would be most susceptible for hydrogen absorption.

Carbon and Sulfur content were determined using combustion infrared detection following ASTM E 1019-08. Hydrogen content was determined through vacuum hot extraction according to ASTM E 146-83. All other components were analyzed by direct current plasma emission spectroscopy according to ASTM E 1097-07.

C.   MICROSTRUCTURE ANALYSIS

1.   Specimen Preparation

A Charmilles Andrew EF630 CNC Wire EDM system using a 0.30 mm diameter cutting wire was used to cut transverse sections across the FSP beads for analysis. These cross-sectional metallographic specimens were cold-mounted using an epoxy resin and prepared using standard processes. The final polish was performed with a water-based 0.05 μm Al_2O_3 suspension on a Buehler ECOMET 3 Variable Speed Grinder/Polisher. The prepared surfaces were then etched with a 5% Nital (5% HNO_3 – 95% Methanol) etchant.

It was noted during polishing that the steel plate was not homogeneous in that several specimens exhibited pitting in the BM, while others did not. This was confirmed later with optical microscopy.

2.   Optical Microscope Imaging

An optical microscope was used to examine the specimens under various magnifications. Several locations were viewed such as BM, TMAZ (advancing side), and SZ. Low-magnification montages were developed to show the entire width of the SZ, left and right TMAZ, as well as BM on either side. Images were post-processed with Adobe Photoshop CS4 in grayscale mode, auto contrast, and auto tone.

3.   SEM Imaging

A Ziess NEON40 SEM was used with field emission electron source operating at 20 keV to examine the specimens under various magnifications. Several locations were viewed, and the results are later depicted in Chapter IV.

D. MECHANICAL TESTING

1. Microhardness

The specimens were removed from their cold molds and repolished to remove scratches from handling during the mold removal. A CSM Instruments MicroCombi Tester with Indentation software was used to micro-indent each specimen to establish a Vickers hardness profile in a grid pattern, as depicted in Figure 4.
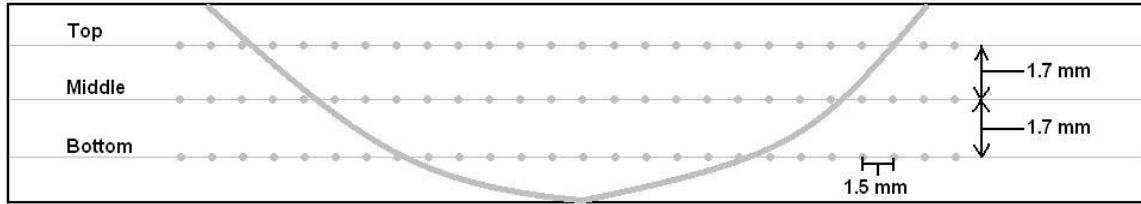
Figure 4.   Depiction of the grid pattern used for microhardness testing. Gray curved line represents SZ general shape.

A test load of 10 N with a 15 sec pause was used with a loading and unloading rate of 20 N/min.

2. Tensile Strength

a. Specimen Preparation

Mini-tensile test specimens were cut such that the tensile axis was centered longitudinally along the FSP beads using the Charmilles Andrew EF630 CNC Wire EDM system. The shape and dimensions of these specimens are shown in Figure 5. The thickness of each specimen varied from 1.0 mm to 1.5 mm due to slight variations in EDM cutting losses as well as polishing.
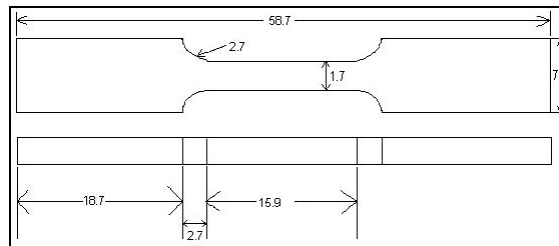
Figure 5.   Mini-tensile specimen dimensions (mm). After [13]

8

b. *Specimen Testing*

Test specimens were sliced to provide two mini-tensile tests for each of several RPM/IPM configurations with the intent on taking the average value between the two tensile tests; there was insufficient FSP material to allow more test specimens. While polishing test specimens, it was noted that there was a crack almost through the gauge width for the 300-4 (wet) and partially through 200-4 (wet) specimens. It was not known whether these cracks were present from the time of FSP, or if they developed during EDM cutting or during polishing.

All tensile tests were performed using an initial strain rate of 2.1×10^{-3}/s. Of all the tensile tests, only two were completed satisfactorily due to slip of the machine grips on the specimens. Only results from the two completed tensile tests (400-2 (dry) and BM) will be discussed later.

THIS PAGE INTENTIONALLY LEFT BLANK

IV.   RESULTS AND DISCUSSION

A.   VISUAL/INITIAL INSPECTION

With the exception of two FSP bead runs, the beads were visually defect-free. The 200-4 (dry) initial run began too hot and ended too cool due to varying the Z-axis force loading. Once a satisfactory load was established, the 200-4 (dry) run was redone and resulted in a visually defect-free bead. The first 300-4 (wet) run produced an excessive amount of flashing (excessive Z-axis force) and was redone with a lower Z-axis force and produced a visually defect-free bead. The plates are shown in Figure 6.

Figure 6.   Post-FSP beads on dry and wet plates showing visually defect-free welds. Rectangular marked areas show cut specimen locations for microscopy analysis.
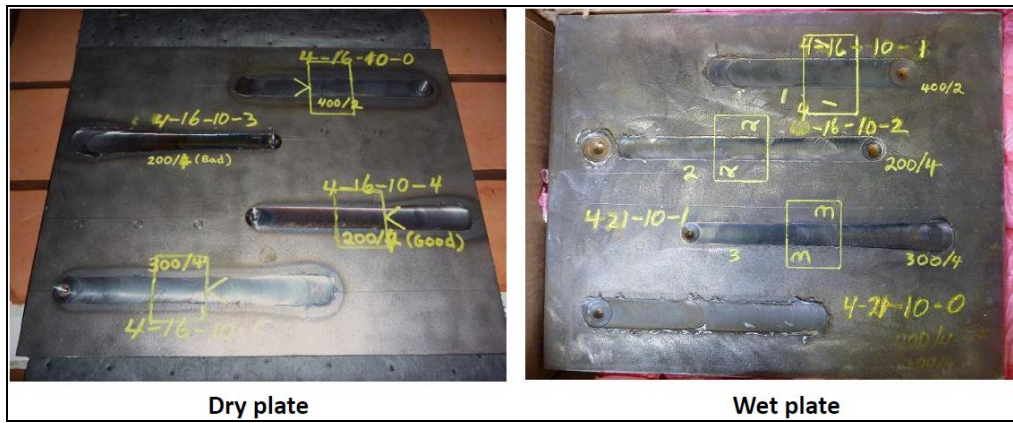
B.   CHEMICAL ANALYSIS

1.   BM Composition

The chemical composition data of the as-received material are shown in Table 2. A comparison of these data with data in the Metals Handbook Vol. 9 [14] revealed that this composition corresponds to AISI 4142 steel.

Table 2.   BM Chemical Composition.

Element	% (weight)
Carbon	0.43
Nickel	0.09
Chromium	0.88
Molybdenum	0.17
Manganese	0.85
Silicon	0.24
Vanadium	0.009
Sulfur	0.029
Phosphorus	0.016

2.   Hydrogen Content

High strength steels' susceptibility to HAC, coupled with current limitations and costly procedures in current fusion welding processes for them, are what make FSW/P such a promising technology.   If FSW/P of high strength steels has any chance of becoming a viable and economical, it must first demonstrate that hydrogen levels of FSW/P beads are within acceptable limits. This is critical especially for the experiments on underwater welding.

MILSPEC maximum hydrogen values in deposited weld metal range from 2.0 to 5.5 ml H_2/100 g metal [15]. The low value of 2.0 was selected to become the maximum permissible hydrogen content in order to be considered a successful FSW/P bead.

Hydrogen content was determined for the BM, 400-2 wet and dry FSP beads. Luvak Inc. reported the results in ppm and where converted to ml/100 g using 1 ml H_2/100 g metal = 0.89 wt-ppm hydrogen in steel [16]. The results are shown in Table 3.

Table 3.   Hydrogen Concentration.

Specimen:	Hydrogen Concentration
Base Metal	0.45 ml/100 g
400-2 (dry)	0.67 ml/100 g
400-2 (wet)	1.24 ml/100 g

A marginal increase in hydrogen was measured for the 400-2 (dry) FSP bead and double that amount measured for the wet bead. However, even this higher value is well below the most conservative limit of 2.0 ml H_2/100 g metal and therefore showed that hydrogen levels were acceptable for the FSP beads. These hydrogen levels were obtained with no shielding gases of any kind, nor with any other hydrogen absorption prevention techniques used. Several studies on FSW/P of steels have used an inert shielding gas to minimize tool oxidation [3, 5, 7, 8, 10, 11, 17] and this would also serve to further minimize hydrogen absorption.

C.   OPTICAL MICROSCOPY

Tunneling defects were observed in the 300 RPM (dry) and 200 RPM (wet and dry) specimens. As the focus of this study is on underwater FSW/P, only the 200 RPM (wet) defect was examined under high magnification.

In order to have comparative results and focus on underwater conditions, each RPM/IPM (wet) FSP bead was closely evaluated. The 400-2 RPM/IPM wet and dry FSP beads were compared with each other to evaluate the effect of water on FSW/P as both produced defect-free beads.

Figure 7 shows low magnification montages for each evaluated FSP bead as well as a higher magnification image of the tunneling defect shown in the 200-4 RPM/IPM bead.
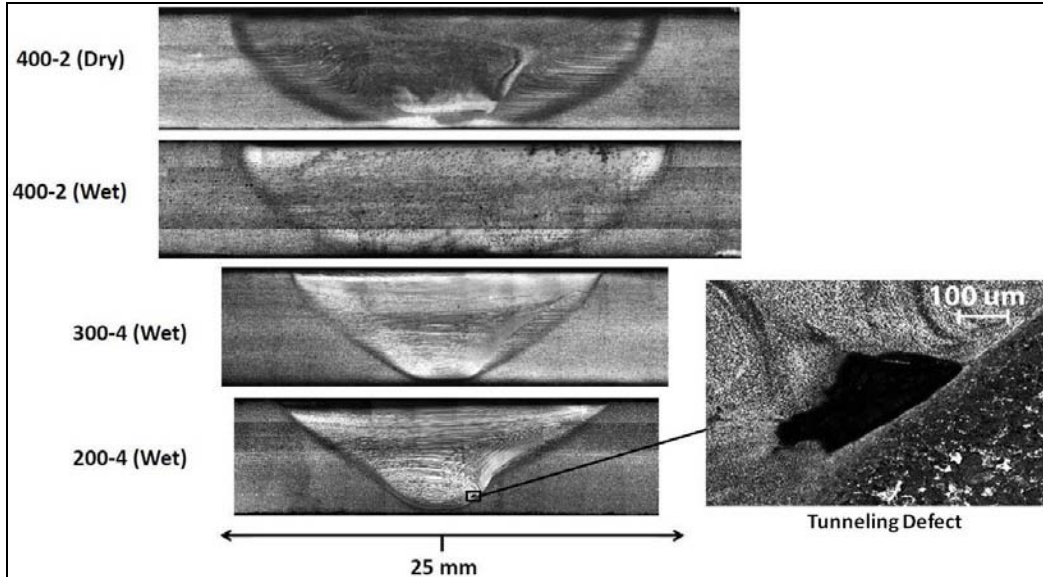
Figure 7.   Low magnification optical microscopy montages of evaluated FSP beads with higher magnification image of 200-4 (wet) tunneling defect. The advancing side is on the right side of the montages and the direction of tool travel is into the page.

As shown in Figure 8, as RPM decreased the volume of the SZ decreased. This was expected as heat input decreases with decreasing RPM and/or with increasing IPM. The notable difference between 400-2 wet and dry beads are the more prominent "flow-bands" in the dry specimen. The shape of the PCBN tool itself can be also discerned from the 400-2 dry specimen.

The 200-4 FSP bead exhibited a tunneling defect on the advancing side, suggesting that 4 IPM was too fast for 200 RPM with this material. These conditions apparently define the lower limit in heat input for this material and tool combination.

During preparation of the specimens, it was noted that the BM was not homogenous; this was confirmed through optical microscopy and can be seen in Figure 8. The 400-2 (dry) specimen showed large voids on the order of 10 μm across, whereas in the 400-2 (wet) specimen, the large voids were on the order of 20 – 30 μm. Both showed a similar amount of impurity inclusions, as well as a banded rolled-grain microstructure from the plate hot-rolling process. The BM consisted of equiaxed grains of ferrite dispersed with pearlite. The ferrite/pearlite content appeared rather non-uniform in different areas of the same plate, as illustrated in Figure 8.

14

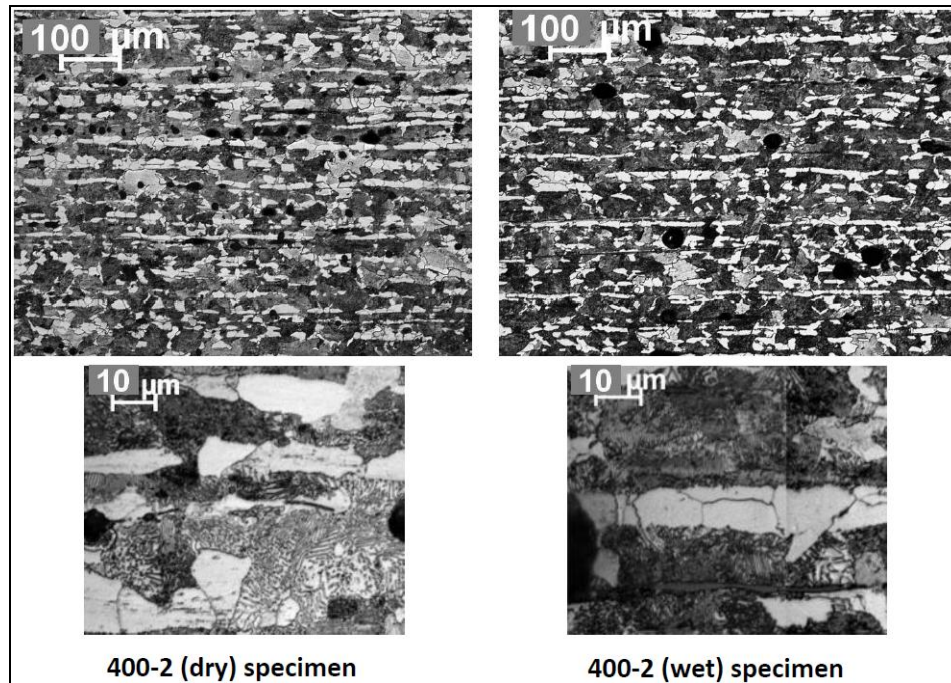Figure 8.   Optical microscopy showing non-homogenous BM between 400-2 dry and wet specimens.

When observed at higher magnification, it was noted that the TMAZ was much broader in the 400-2 (dry) compared with 400-2 (wet). This is shown in Figure 9.
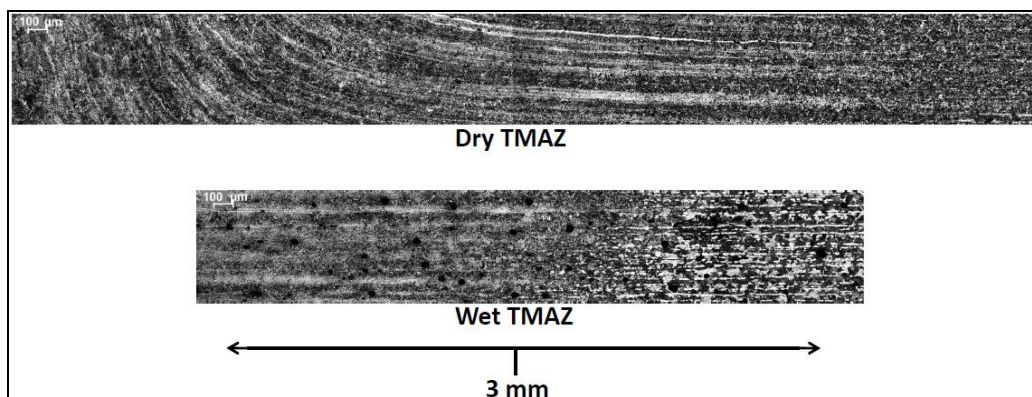

Figure 9.   Optical microscopy showing 400-2 (dry) and 400-2 (wet) TMAZs. The advancing side is on the right side of the montages and the direction of tool travel is into the page.

The martensitic microstructures in the SZ under both dry and wet conditions suggest that the samples were fully austenitized during the FSP runs and rapidly quenched. The micrographs in Figure 10 suggest that the martensitic structures are much finer under the wet conditions. This suggests that (a) the temperature achieved during the dry condition was higher than that during the wet conditions leading to finer austenite grain size in the latter samples and/or (b) the quenching rate subsequent to FSP was higher under the wet condition. This is in agreement with the observations of higher temperatures during dry FSP runs.
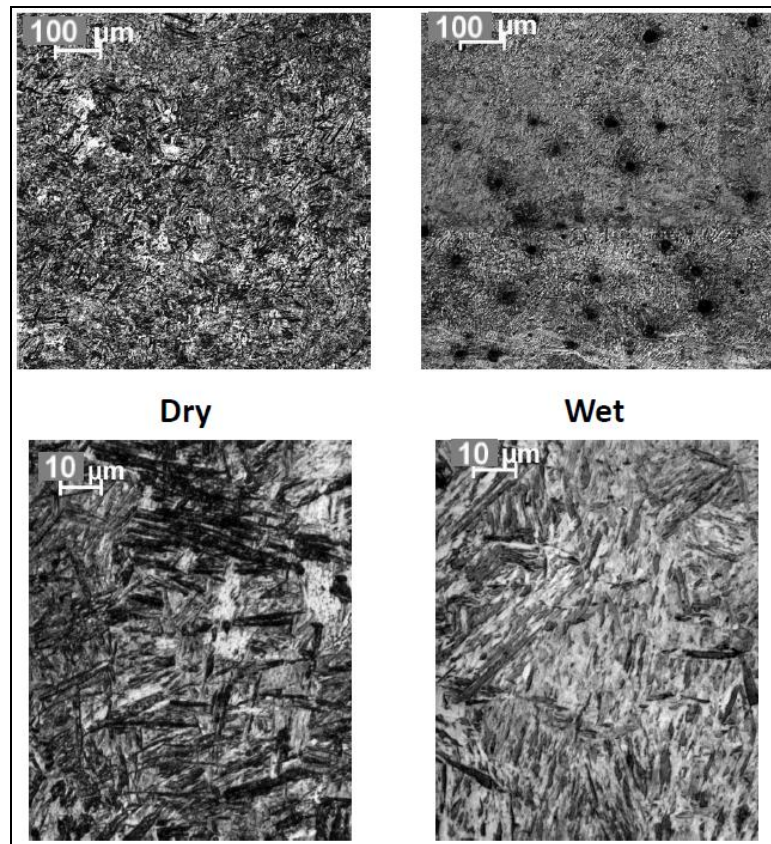
Figure 10.   Optical microscopy showing 400-2 (dry) and 400-2 (wet) SZ. Of note, the higher number of micro-voids in the wet specimen was due to the BM having more (and larger) micro-voids than BM in the dry specimen.

As the RPM for the wet specimens was lowered, the TMAZ displayed more "flow-bands" and can be seen in Figure 11.
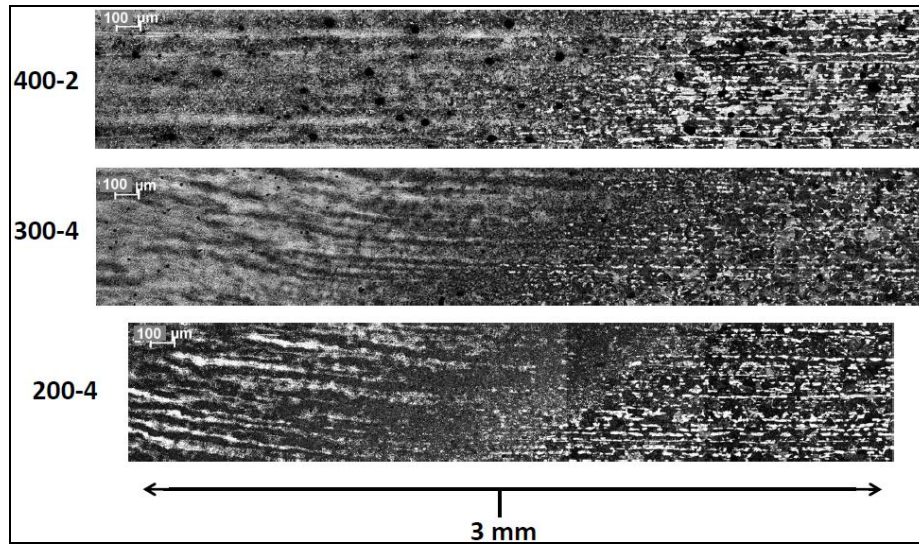
Figure 11.   Optical micrographs showing different RPM (wet) FSP bead TMAZs. The advancing side is on the right side of the montages and the direction of tool travel is into the page.

The center of the SZ was observed for each wet RPM/IPM FSP bead and is shown in Figure 12.
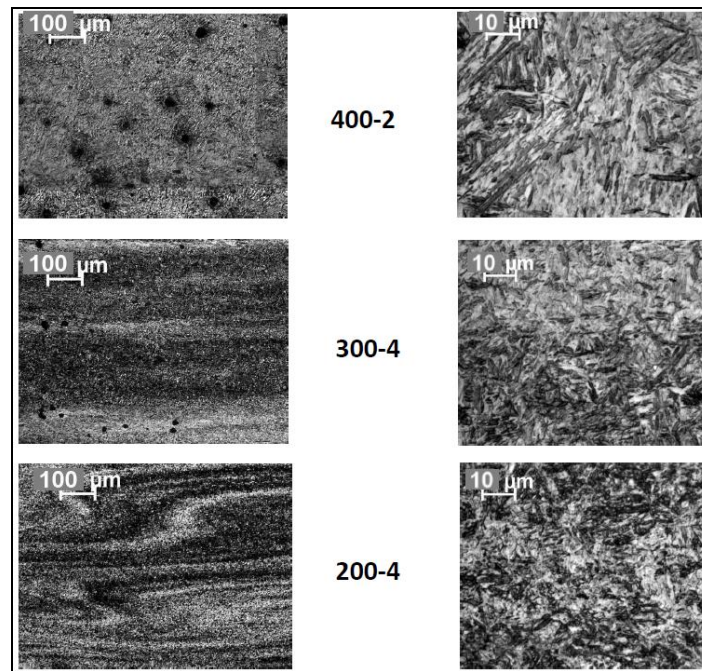
Figure 12.   Optical micrographs showing the microstructures observed in different RPM (wet) FSP bead SZs. Lower magnification micrographs are shown on the left and higher magnification micrographs on the right.

At lower magnifications (Figure 10, left), there was a noticeably different microstructure for each bead. At 400 RPM, the martensitic microstructure was homogenous, but as the RPM decreased, there were bands of martensite mixed with ferritic or carbide bands. The 200 RPM sample showed the most banding and also showed a swirl pattern. As shown in the higher magnification micrographs (Figure 10, right), all of these FSP RPM conditions led to austenitization and subsequent martensitic transformation. It appeared that the martensitic units were more fine as the RPM was decreased (and thus lower heat input), which suggested that the temperatures achieved were lower. In addition, the 200-4 specimen exhibited a tunneling defect and would not be considered an acceptable weld.

D.   SEM MICROSCOPY

Several locations were observed under the Zeiss NEON40 SEM and these are depicted on Figure 13.
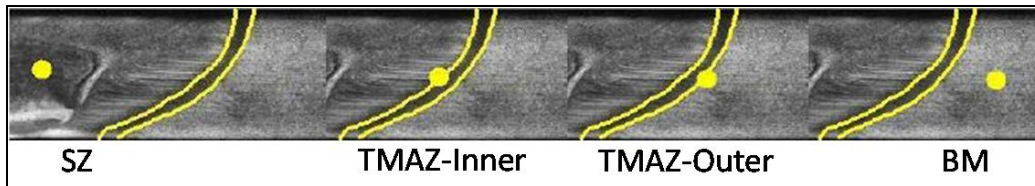
Figure 13.   SEM viewing locations represented with yellow dots. The advancing side is shown with FSP travel into the page.

Dry and wet 400-2 FSP beads were examined to document differences in microstructure attributable to underwater FSP. At higher magnifications, there seemed to be little difference in microstructure between the two specimens. The notable difference between the two was seen at lower magnifications with the dry specimen showing more prominent "flow-bands" and showing the outline of the tool tip.

Figure 14 compares SEM images for 400-2 (wet and dry) FSP beads for TMAZ-Inner and Outer locations. Both conditions showed similar microstructures for each location. At the TMAZ-Outer location, a primarily pearlitic microstructure with

randomly oriented and dispersed ferrite grains was observed. This microstructure was similar to the BM except that some of the lamellar pearlite was distorted in the TMAZ-Outer location.

Observed in TMAZ-Inner locations for both conditions was what appeared to be the start of a martensitic microstructure interspersed with pearlite. Few, if any, ferrite grains were observed over several SEM micrographs.
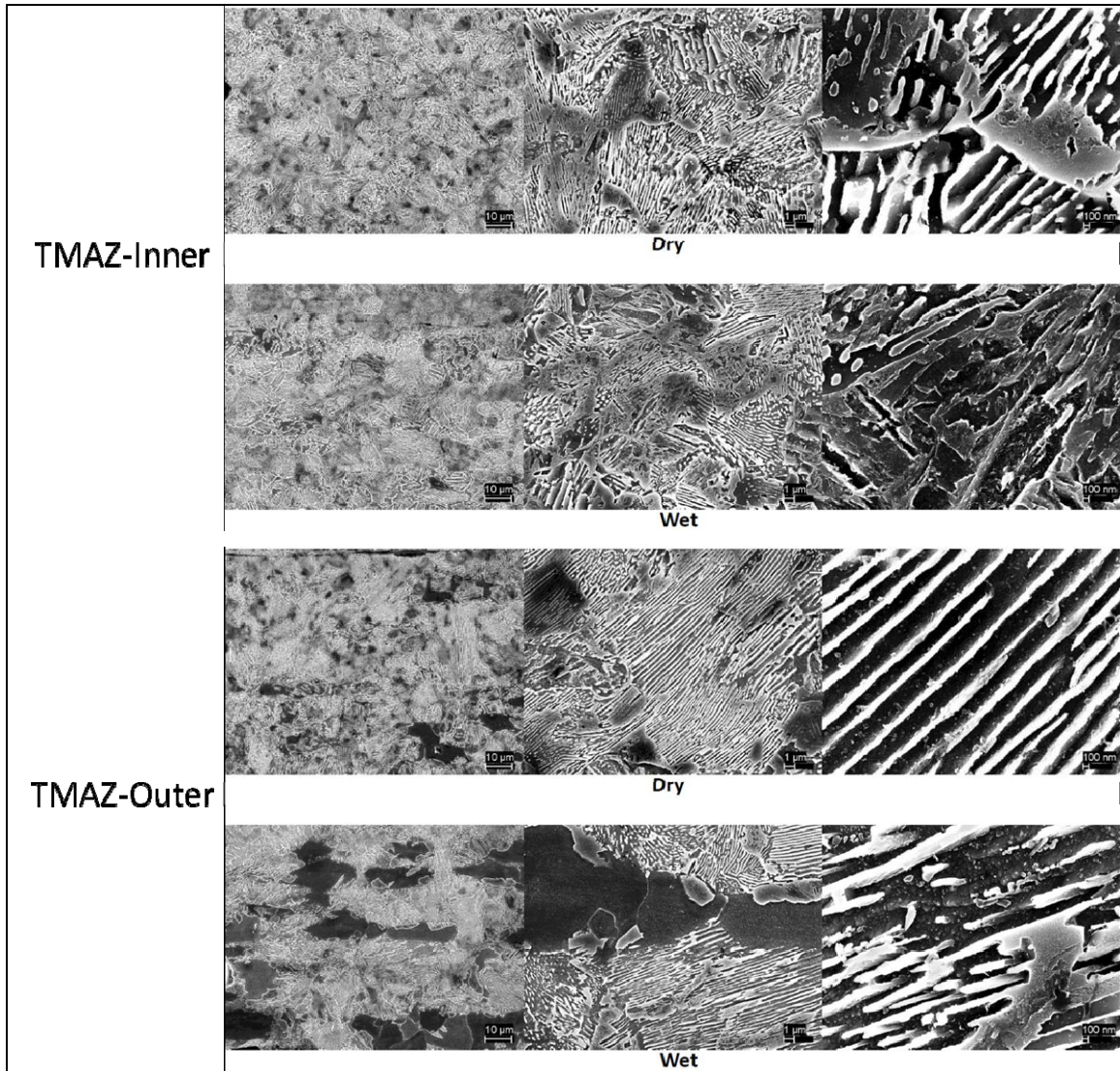

Figure 14.   SEM micrographs of TMAZ-Inner and Outer locations for 400-2 wet and dry FSP beads. From left to right scale bars read 10 μm, 1 μm, and 100 nm.

SEM micrographs taken at the center of the SZ showed essentially the same microstructure in both dry and wet FSP conditions. This microstructure was clearly martensitic and homogenous and is shown in Figure 15.
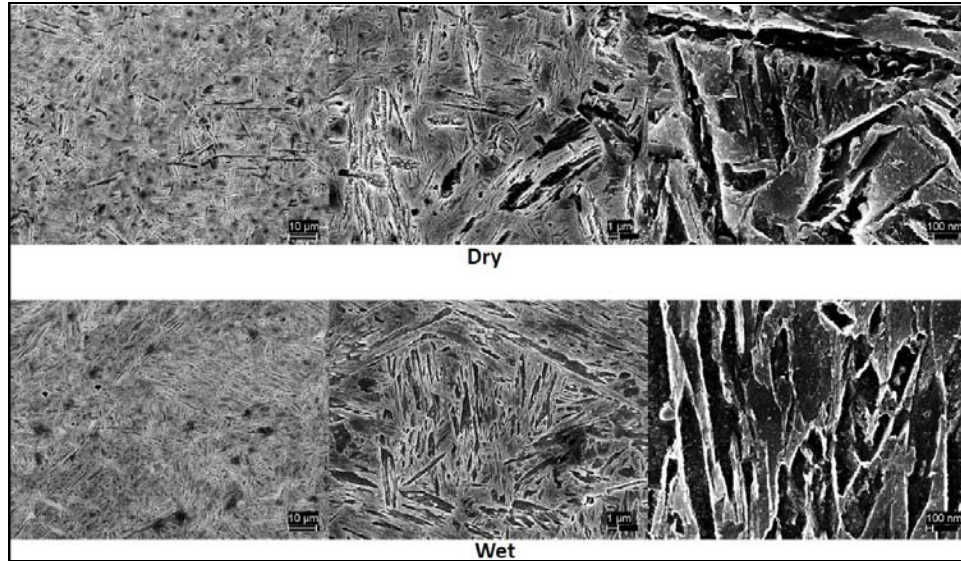

Figure 15.   SEM micrographs of SZ locations for 400-2 wet and dry FSP beads. From left to right scale bars read 10 μm, 1 μm, and 100 nm.

That the SEM micrographs showed very similar microstructures between wet and dry 400-2 FSP beads demonstrated that while the tool temperatures were distinctly different, the resulting microstructural constituents were essentially the same as expected.

Next observed was a comparison between 400-2 and 200-4 (both wet) FSP beads. Figure 16 compares SEM images for TMAZ-Inner and Outer locations. Both conditions showed similar microstructures for the TMAZ-Outer location; primarily pearlitic with randomly oriented and dispersed ferrite grains. At the TMAZ-Inner location, SEM micrographs revealed that the 200-4 FSP bead had many voids. Other than the voids, the microstructures for both 400-2 and 200-4 FSP beads were similar in that distorted pearlite was interspersed with martensite. These observations suggest that there was incomplete austenitization in these TMAZ regions due to the lower temperatures achieved in such regions during FSP.
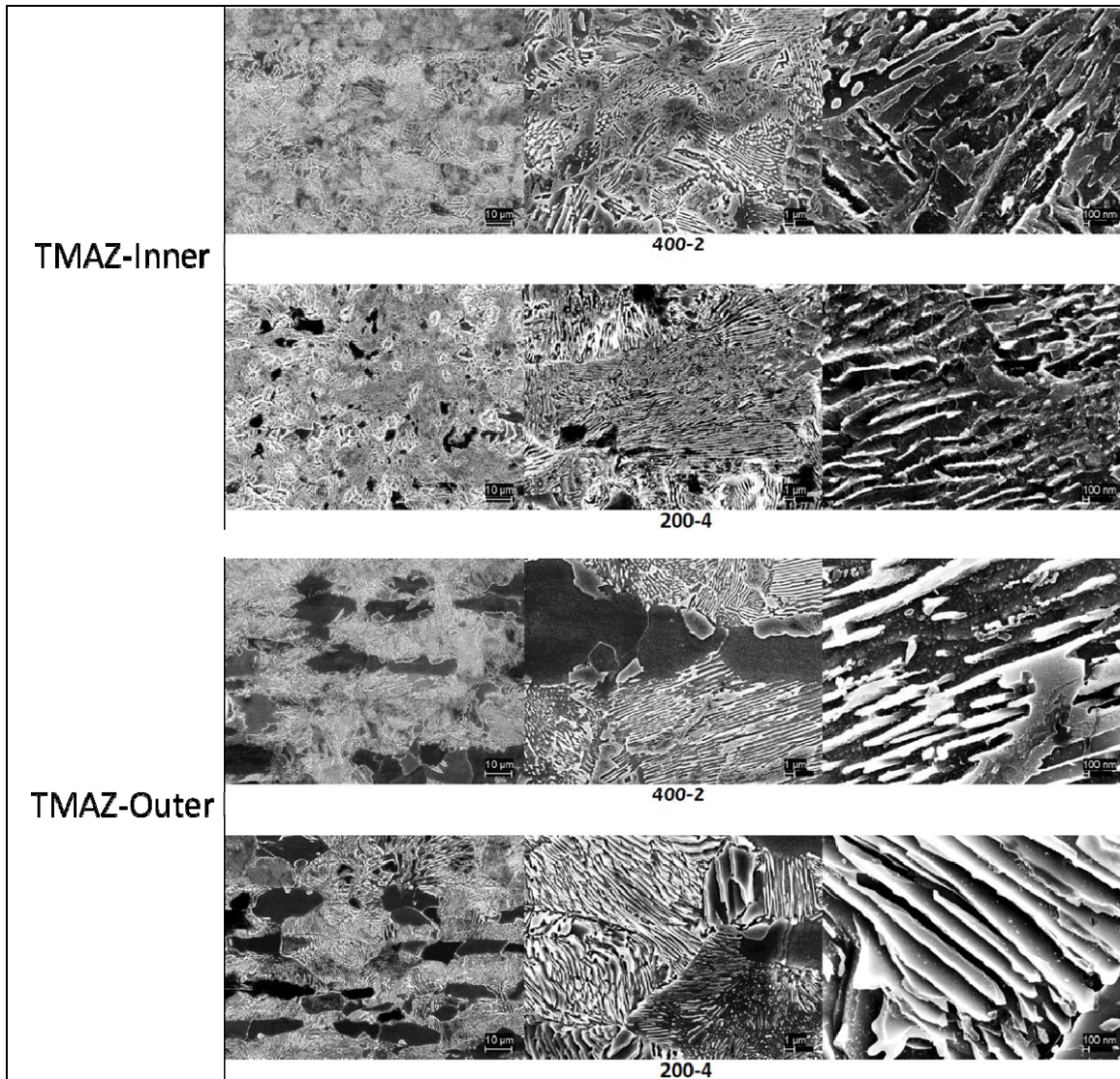
Figure 16.   SEM micrographs of TMAZ-Inner and Outer locations for 400-2 and 200-4 wet FSP beads. From left to right scale bars read 10 μm, 1 μm, and 100 nm.

SEM micrographs taken at the center of the SZ of both 400-2 and 200-4 FSP beads showed essentially the same microstructure. This microstructure was clearly martensitic and homogenous and is shown in Figure 17.
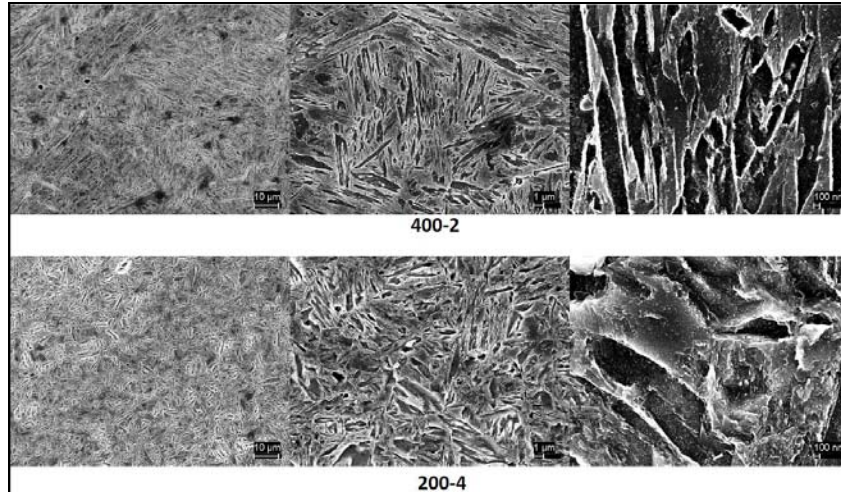
Figure 17.   SEM micrographs of SZ locations for 400-2 and 200-4 wet FSP beads. From left to right scale bars read 10 μm, 1 μm, and 100 nm.

Figure 18 was compiled to give a more complete view of the transformation process that was observed starting with the BM through the SZ. These micrographs were taken of the 400-2 (wet) FSP bead and show the most promising RPM/IPM combination for underwater FSW/P of 4142 steel.
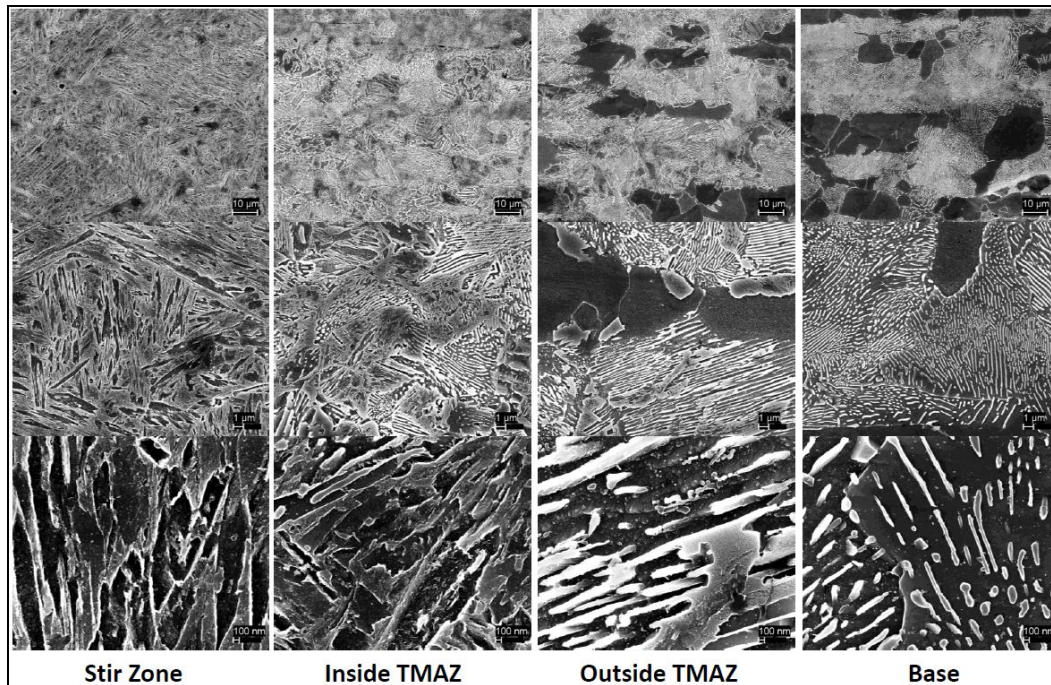

Figure 18.   SEM micrographs of each location for 400-2 wet FSP bead. From top to bottom scale bars read 10 μm, 1 μm, and 100 nm.

E.   MECHANICAL PROPERTIES

Mechanical properties of the FSP samples were evaluated by determining the microhardness variations in various samples across the SZ at various depths from the sample surfaces in the transverse sections of the metallographically prepared samples. Preliminary tensile tests were also carried out. The results from these studies are discussed below.

1.   Microhardness

Vickers microhardness values of the BM ranged from 143 HV to 242 HV. Clearly, this variation was due to the defective and inhomogeneous structure (inclusions, porosities, pearlite content variations) of the alloy plate studied here. Of note, the lower values for microhardness were obtained on the 400-2 (wet) FSP bead specimen that contained the highest amounts of voids and inclusions of all the specimens. For comparative analysis, the microhardness test data was compared between the 400-2 wet and dry FSP beads and then between the 400-2 and 200-4 (wet) FSP beads. The resultant plots are presented as Figure 19. The corresponding low magnification micrographs are also included in this figure.
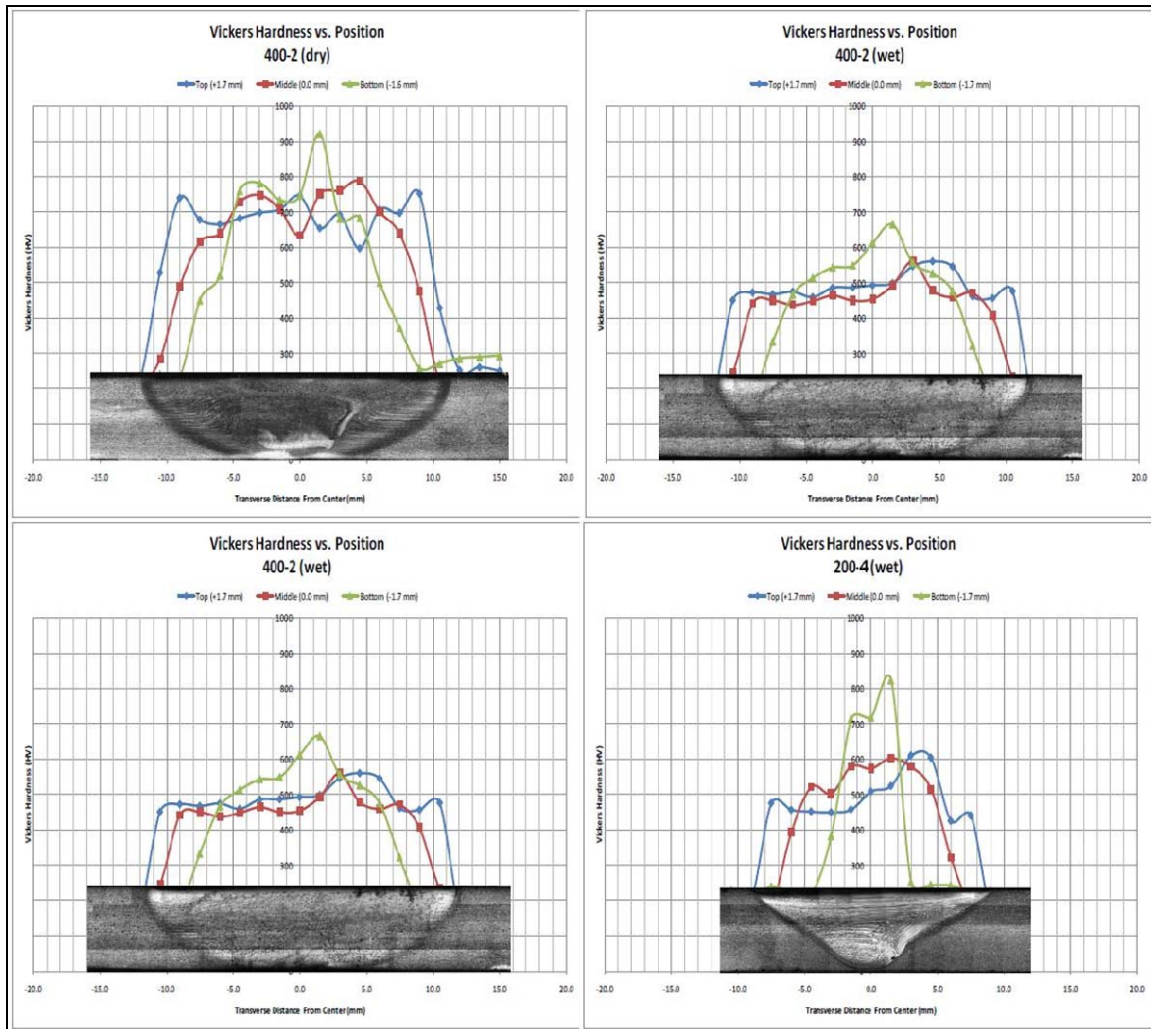
Figure 19.   Vickers microhardness plots. Vertical scale HV from 300 (visible) to 1000. Horizontal scale distance from 0.0 (center) to +/- 20.0 mm. Montage overlays are to scale.

The apparent difference of approximately 200 HV between 400-2 dry and wet FSP bead average microhardness is somewhat offset due to the wet specimen having started with an average microhardness of 100 HV less in the BM. That there still is an average microhardness of 100 HV higher for the dry FSP bead could be due to the poorer quality BM that the wet FSP bead started with. Both beads produced martensitic microstructures, but it is unclear as to why the dry FSP bead would have a higher microhardness than the wet FSP bead. This is contrary to the expectation that with an underwater FSP bead the cooling rate would be greater, and therefore better able to

24

produce finer martensite. The other possibility is that the dry FSP bead reached a much higher peak temperature, and as a result, would have a high cooling rate after being fully austenitized. However, both optical and SEM micrographs showed a fully martensitic microstructure in the SZ. Variations in carbon content of the as-received plate was the most likely reason for such large variations in the martensitic hardness observed in different samples.

The 200-4 Bottom row of microhardness data points produced an unexpectedly high HV value that was approximately 200 HV higher than the other rows and the average value for 400-2. Once the low-magnification montage of the 200-4 FSP bead was overlaid onto the microhardness plot, it was clear that the higher values corresponded to concentrated (as shown by brighter white on the montage) areas of martensite.

The increase in microhardness coupled with optical and SEM micrographs left no doubt that martensite was formed during each configuration tested. Thus all the microstructural observations and microhardness measurements consistently indicated that temperature increases during FSP was sufficient to fully austenitize the steel and that the subsequent cooling rate was sufficient to induce the martensitic transformations in the alloy.

2. Tensile Strength

Tensile testing resulted in just two complete sets of good data due to the tensile test specimens slipping in the gripped regions during the tests. These two sets were for the BM and the 400-2 (dry) FSP bead. The material hardness coupled with small size made testing difficult, if not impossible with the equipment that was available at the time. The resulting plots are shown in Figure 20. The BM exhibited a typical steel stress-strain curve associated with a ferrite-pearlite microstructure, while the FSP bead showed a brittle, yet strong, material typical of martensitic microstructure. Given that the use of the material in structures would ordinarily mean that operating conditions would fall below the yield point of the base material, the FSP bead material would not fail prior to the BM.
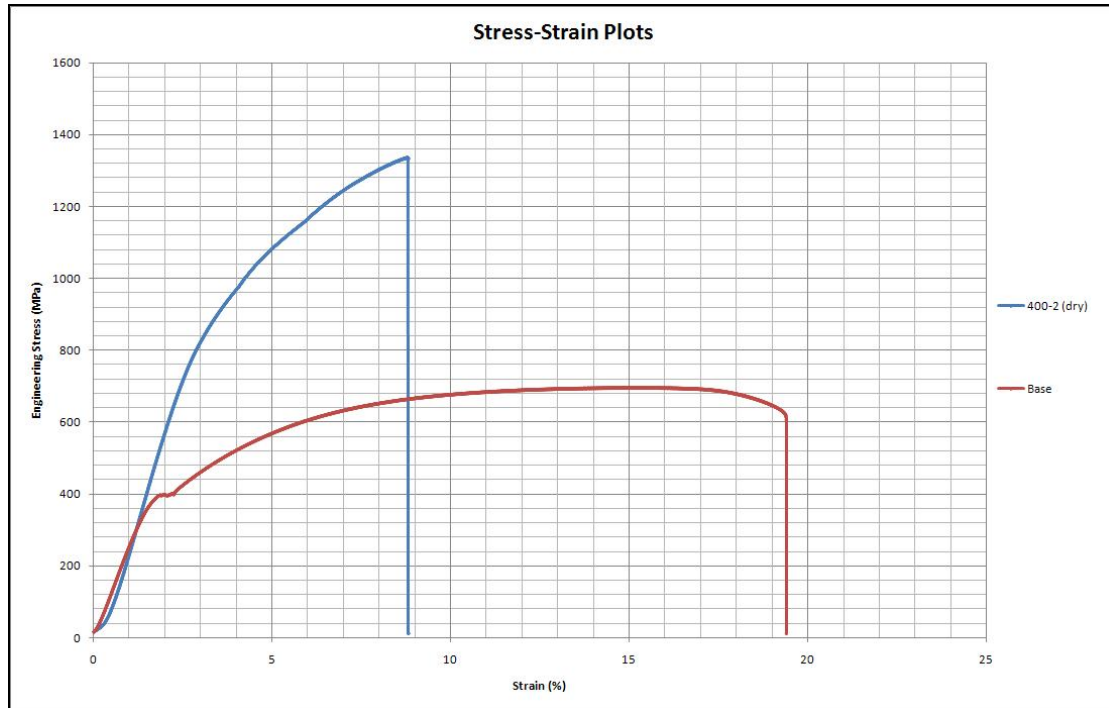
25

Figure 20.   Engineering stress vs. Strain for 400-2 (dry) in blue and BM in red.

V. CONCLUSIONS

A. SUMMARY OF THIS WORK

In this work, preliminary studies on the feasibility of underwater FSP of a hardenable alloy steel were carried out.

1. To our knowledge, this forms the first underwater FSP study and in particular on a hardenable alloy steel. The feasibility of underwater FSW/FSP of hardenable alloy steel has thus been demonstrated.

2. Hydrogen concentration in FSP bead material for both dry and underwater conditions was well within acceptable levels for high strength steel welds.

3. A martensitic microstructure was formed in the SZ for the RPM/IPM combinations tested. A correspondingly high microhardness was observed in the SZ along with a significantly higher tensile strength.

4. Defect-free FSP beads were accomplished for three configurations: 400-2 (dry), 400-2 (wet), and 300-4 (wet).

These conclusions support the promising future for underwater FSW of hardenable alloy steels. Further research is needed to establish alloy-specific operating parameter "windows" and to further evaluate mechanical properties of the FSW/P material.

B. FUTURE RESEARCH

1. The logical next step to support Navy-specific use of underwater FSW of hardenable alloy steel would be to perform a similar experiment on HY-80 or HY-100 plate. To more accurately reflect real-world conditions, it is recommended that the water used for the wet conditions be seawater or simulated seawater or a 3.55 NaCl solution. The increased salinity could affect the cooling rate and therefore the microstructure. The beads should be longer than eight inches (20 cm) or there should be more than one bead for each condition. This would support more FSP bead material for mechanical testing,

specifically tensile strength testing. The tabs on the tensile specimen should be longer to account for grip size on the tensile testing machine to minimize the possibility for slipping.

2.   The use of a shielding gas should be evaluated for both tool longevity consideration as well as further minimizing hydrogen absorption.   Another potential benefit of using a shielding gas underwater would be that cooling rates immediately following the FSW/P would be lower and therefore provide a means for controlling the microstructure formation.

3. Higher RPM configurations should be evaluated to determine the resulting Z-axis force needed to produce the FSW/P beads. A lower force is desired so that the portable machine will have less force to account for in its design.

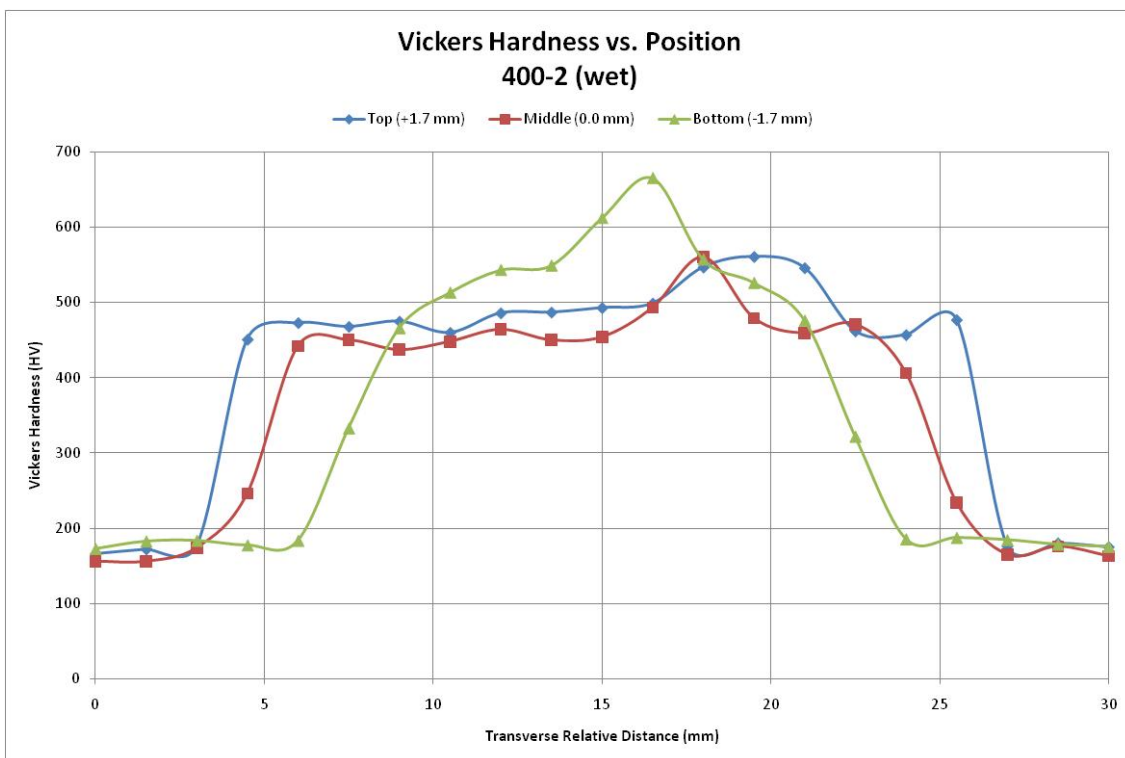# APPENDIX A – ADDITIONAL FIGURES

These figures are included to provide higher resolution pictures for clarification.
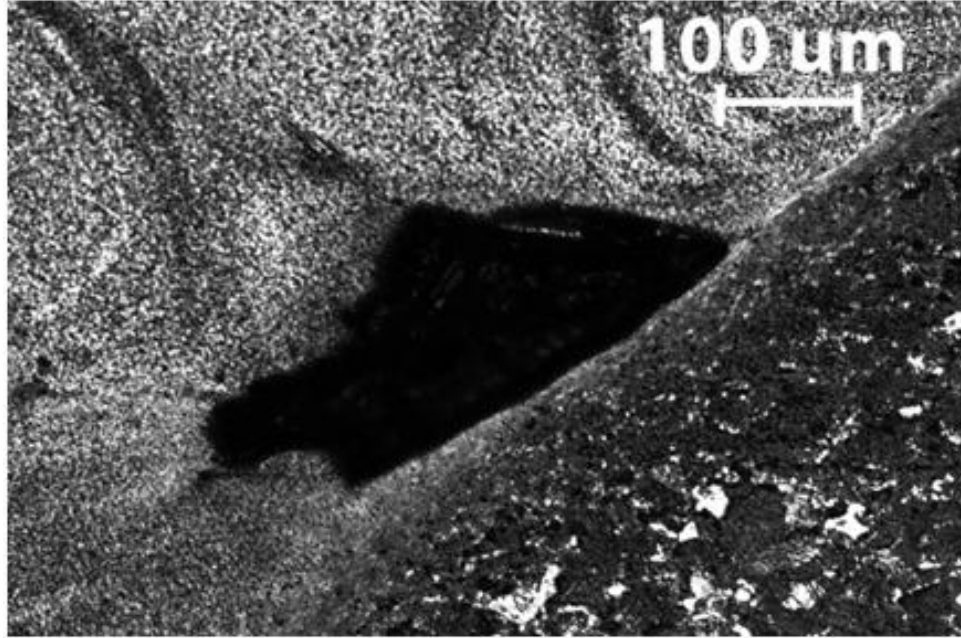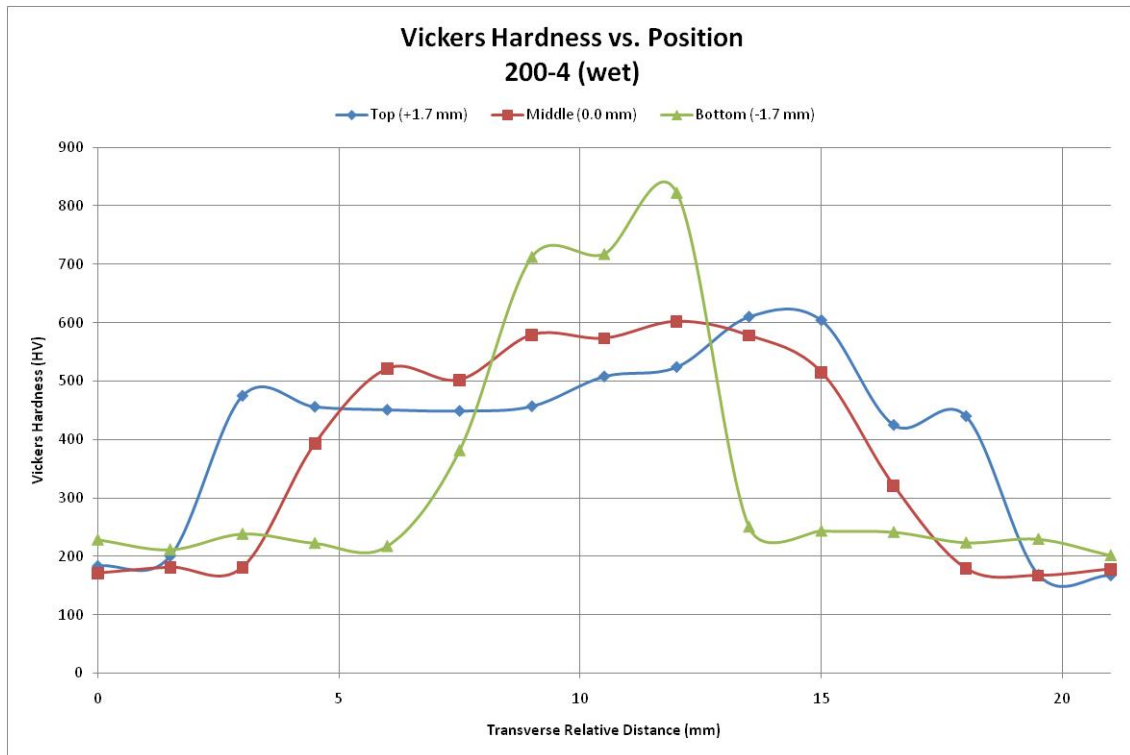

Optical micrograph showing the tunnel defect in the 200-4 (wet) FSP bead.
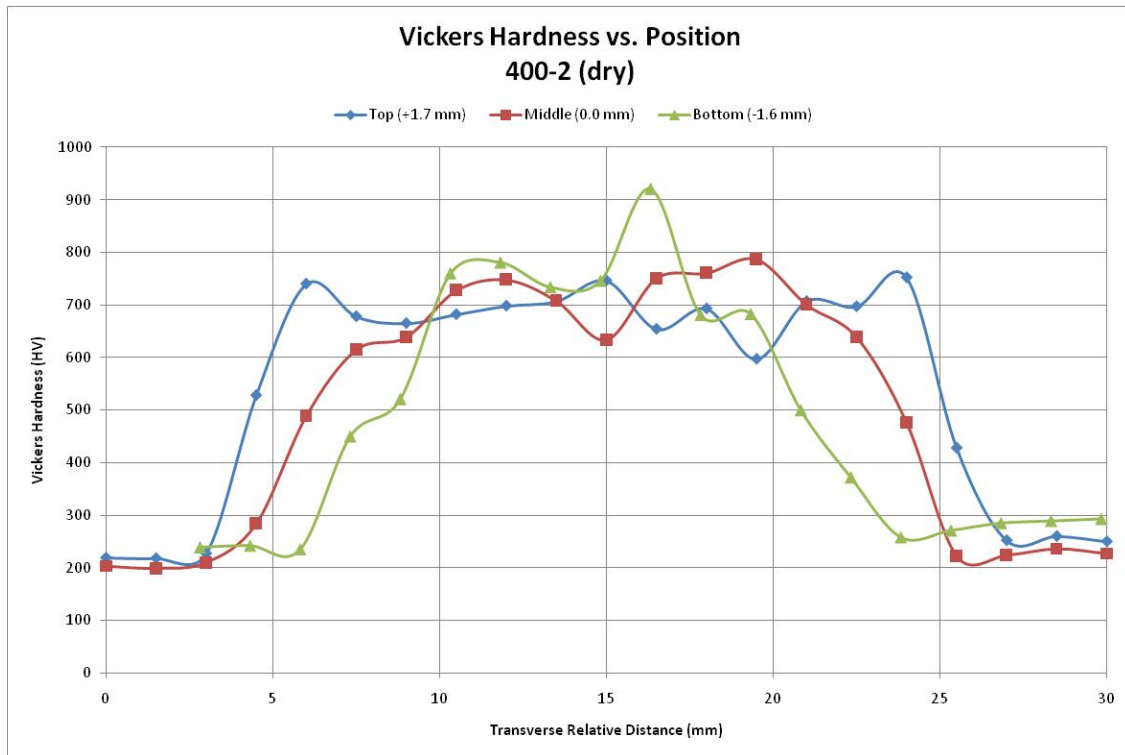
Microhardness plot for 400-2 (dry) FSP bead

Microhardness plot for 400-2 (wet) FSP bead

Microhardness plot for 200-4 (wet) FSP bead

THIS PAGE INTENTIONALLY LEFT BLANK

APPENDIX B – LUVAK INC. REPORT

Luvak Inc.
722 Main Street
P.O. Box 597
Boylston, MA 01505
Phone 508-869-6401
www.luvak.com

Analytical report no.
0-57749
Page 1 of 1

Requested by:
Naval Postgraduate School
1 University Circle
Monterey, CA 93943

Attention:
LT Norm Overfield, USN
normusn@gmail.com

Invoice number: 64195
Customer Purchase Order no.: Credit Card

Date received: 06/07/10
Report date: 06/21/10
Invoice date: 06/21/10

Description: Three samples were analyzed as listed below.

Results:

Sample Identification	Base ppm	Wet ppm	Dry ppm
Hydrogen	.4	1.1	.6
	%		
Chromium	.88	---	---
Manganese	.85	---	---
Molybdenum	.17	---	---
Nickel	.092	---	---
Phosphorus	.016	---	---
Silicon	.24	---	---
Vanadium	.009	---	---
Carbon	.427	---	---
Sulfur	.029	---	---

Methods: Carbon & Sulfur - Combustion infrared detection - ASTM E 1019-08
Hydrogen - Vacuum hot extraction - ASTM E 146-83
All others - Direct current plasma emission spectroscopy - ASTM E 1097-07

Luvak Inc.

By

Dean C. Gaskill
Vice President/General Manager

THIS PAGE INTENTIONALLY LEFT BLANK

LIST OF REFERENCES

[1]   K. Masubuchi and D. C. Martin, "Mechanisms of Cracking in HY-80 Steel Weldments," *Welding Journal,* vol. 41, pp. 375S-384S, 1962.

[2]   J. H. Nixon, "Underwater repair technology," pp. 108, 2000.

[3]   R. S. Mishra, "Friction stir welding and processing," *Materials Science Engineering.R, Reports,* vol. 50, pp. 1, 2005.

[4]   H. Fujii, "Friction stir welding of carbon steels," *Materials Science Engineering.A, Structural Materials,* vol. 429, pp. 50–57, 2006.

[5]   Y. S. Sato, "Microstructural evolution of ultrahigh carbon steel during friction stir welding," *Scr. Mater.,* vol. 57, pp. 557–560, 2007.

[6]   T. Huang, "Microstructural evolution of DP980 steel during friction bit joining," *Metallurgical and Materials Transactions A Physical Metallurgy and Materials Science,* vol. 40, pp. 2994–3000, 2009.

[7]   Y. C. Chen, "Evaluation of microstructure and mechanical properties in friction stir processed SKD61 tool steel," *Mater Charact,* vol. 60, pp. 1471–1475, 2009.

[8]   S. H. Aldajah, "Effect of friction stir processing on the tribological performance of high carbon steel," *Wear,* vol. 267, pp. 350–355, 2009.

[9]   L. Cui, "Friction stir welding of a high carbon steel," *Scr. Mater.,* vol. 56, pp. 637, 2007.

[10]   A. Ozekcin, "A microstructural study of friction stir welded joints of carbon steels," *Int. J. Offshore Polar Eng.,* vol. 14, pp. 284, 2004.

[11]   Y. D. Chung, H. Fujii, R. Ueji and N. Tsuji, "Friction stir welding of high carbon steel with excellent toughness and ductility," *Scr. Mater.,* vol. 63, pp. 223–226, 7, 2010.

[12]   K. M. Richmond. (2010). RE: Assistance needed on welding questions. *Email correspondence from branch head for Code 250 - Submarine Structural, Puget Sound Naval Shipyard*.

[13]   B. P. Rosemark and Naval Postgraduate School, "Friction stir processing parameters and property distributions in cast nickel aluminum bronze," pp. 51, 2006.

[14]   American Society for Metals, Metals Park,OH (USA).HandbookComittee., *Metals Handbook. Vol. 9 : Metallography and Microstructure,* pp. 177, Metals Park, OH (USA): AMS, 1985.

[15]   Military Specification, "MIL-E-23765/2E," pp. 10, 1994.

[16]   I. Maroef, "Hydrogen trapping in ferritic steel weld metal," *International Materials Reviews,* vol. 47, pp. 191–223, 2002.

[17]   T. J. Lienert, "Friction stir welding studies on mild steel," *Welding Journal,* vol. 82, pp. 1–9, 2003.

INITIAL DISTRIBUTION LIST

1. Defense Technical Information Center
   Ft. Belvoir, Virginia

2. Dudley Knox Library
   Naval Postgraduate School
   Monterey, California

3. Engineering and Technology Curricular Office
   Naval Postgraduate School
   Monterey, California

4. Professor Terry R. McNelley
   Naval Postgraduate School
   Monterey, California

5. Professor Sarath Menon
   Naval Postgraduate School
   Monterey, California